EuroIntervention

IVUS beyond the horizon

Antonius F.W. van der Steen[1,2]*, Radj A. Baldewsing[1], F. Levent Degertekin[3], Stanislav Emelianov[4], Martijn. E. Frijlink[1], Yuji Furukawa[5], Dave Goertz[1,2], Mustafa Karaman[6], Pierre T. Khuri-Yakub[7], Kang Kim[8], Frits Mastik[1], T. Moriya[9], Ömer Oralkan[7], Yoshifumi Saijo[10], Johannes A Schaar[1], Patrick W Serruys[1], Shriram Sethuraman[4], Akira Tanaka[11], Hendrik. J. Vos[1,12], Russell Witte[8], Matthew O'Donnell[8]

1. Biomedical Engineering, Thorax Center Erasmus MC, Rotterdam, The Netherlands; 2. Interuniversity Cardiology Institute of the Netherlands; 3. Georgia Institute of Technology, Atlanta, Georgia, USA; 4. Department of Biomedical Engineering, The University of Texas at Austin, USA; 5. Tokyo University of Agriculture and Technology, Tokyo, Japan; 6. Isik University, Istanbul, Turkey; 7. E. L. Ginzton Laboratory, Stanford University, Stanford, California, USA; 8. Department of Biomedical Engineering, Univ. of Michigan, Ann Arbor, USA; 9. Tokyo Metropolitan University, Tokyo, Japan; 10. Institute of Development, Aging and Cancer, Tohoku University, Sendai, Japan; 11. Faculty of Symbiotic Systems Science, Fukushima University, Fukushima, Japan; 12. Seismics and acoustics, Technical University Delft, The Netherlands

Introduction

Intravascular Ultrasound is a clinically available technique that can image the vessel wall and atherosclerotic plaque[1]. Although the first patent on this technique dates from 1972[2,3], the first catheters for clinical use were only available in the late eighties[4,5]. Since then this diagnostic technique is ever evolving. The main clinical applications to date have been assessment of free lumen and atherosclerotic plaque area[6], volume and therapy guidance[7,8] and guidance of stent placement[9]. To a lesser extent, it has been used for dosimetry in brachytherapy[10] and for assessing the true 3D orientation of coronary arteries and plaque to perform haemodynamic and shear stress studies[11-13].

At present, IVUS has only been used to a limited percentage of its potential. Most concepts mature outside the view of a clinical audience, but are widely discussed in the technical ultrasonics and biomedical engineering societies before they become available products. Probably the most appropriate platform for this has been the annually held IEEE Ultrasonics Symposium. Most IVUS equipment and signal processing methods were discussed here long before they became available in the clinic[14,15]. The array catheter and its beam forming were introduced in 1991[16]. Also forward looking IVUS has been discussed by several groups[17,18]. Qualitative flow[19,20] and quantitative flow[21-23] assessment derived from IVUS data were introduced here as well as tissue characterization using RF data, now available under the name Virtual Histology[24-27]. Also IVUS Elastography, Palpography and tissue velocity imaging[28-32] were nurtured at this symposium.

This paper gives a review of IVUS techniques under development that were discussed at the 2005 IEEE Ultrasonics symposium. Although not all will become products, it gives a good impression of what is cooking in engineering kitchens.

Forward-Viewing IVUS using CMUTs

Forward-viewing ultrasound volume images are desired for many intravascular and intracardiac applications such as guiding treatment of chronic total occlusion, helping stent deployment, and monitoring ablation procedures in the heart. Because of the requirements for a guidewire in catheters, an annular ring is the preferred geometry for transducer arrays. However, it is very challenging to implement this geometry in a very small scale (1-2 mm) using existing piezoelectric transducer technology[18].

** Corresponding author: Biomedical Engineering, Thorax Center Ee 23.02, Erasmus MC Rotterdam, P.O. Box 1738, 3000 DR Rotterdam, The Netherlands*

E-mail: a.vandersteen@erasmusmc.nl

Capacitive Micro-machined Ultrasonic Transducers (CMUT) are transducers that consist of many tiny air filled capacitors, with a flexible electrode membrane on top. When a DC bias voltage is applied to these miniature membrane transducers a stress is developed proportional to the voltage applied squared and the top electrode membrane deflects. Operationally they show a lot of similarity to piezoelectric materials, but they do have a few distinct advantages.

CMUT arrays can be made in any arbitrary geometry with very small dimensions using photo-lithographic techniques and standard micro-fabrication processes. In addition to their ease of fabrication, CMUTs also offer performance advantages such as wide bandwidth and improved sensitivity[33]. CMUTs are also particularly suited for high frequency arrays because the fabrication process used is routinely able to produce features several microns in size. Recent developments in micro-machined ultrasound transducer technology have enabled implementation of IVUS arrays for forward-looking imaging at the tip of a catheter[17,34]. This technology is currently implemented by a group from Stanford[35] and a group from Georgia Tech[36].

At Stanford, a 64-element, 2-mm diameter CMUT ring array allows full synthetic phased array volumetric images to be generated with integrated electronics (Figure 1a).

At Georgia Institute of Technology, a similar array with a 1.15 mm diameter has been constructed[37-38]. (Figure 1bc)

An interesting feature of CMUT operation is the ability to change the operating frequency by changing the DC bias. If the DC bias is made so high that the upper membrane just touches the lower, the so called collapse mode, the membrane cannot vibrate any more at its fundamental resonance frequency and it will vibrate at harmonic frequencies. The resulting operating frequencies in conventional and collapse regimes for these arrays can be e.g. 8.5 MHz and 19 MHz, respectively. Potentially, this operating flexibility of CMUTs allows on-demand switching between its two modes of operation during the imaging procedure, thereby providing a choice between the low frequency conventional mode with high penetration for navigation and the high frequency collapse mode with high resolution for diagnosis. The imaging capacity of forward looking arrays is shown in Figure 2. Phantoms including deployed and undeployed forms of a Palmaz-Schatz coronary stent have been imaged.

It should be understood that such elements have not been mounted on a catheter yet. Minimization and integration of electronics are the main challenges in the near future.

Ultrasonic micromotor for IVUS

Commercially available IVUS catheters contain either 64 static elements or one rotating element. An advantage of a single element is that it is larger, and thus it is easier to obtain a good signal to noise ratio or achieve higher frequencies, resulting in a higher resolution. One of the disadvantages of a mechanically rotating IVUS systems is non-uniform rotational distortion (NURD)[31,39], caused by the long flex between the ultrasound element and the motor driving it. NURD can be overcome by rotating a transducer or a mirror using a micro motor placed close to them. The feasibility of an electromagnetic micromotor for IVUS has been shown in the past[40,41]. Given that metallic structures are potentially present in the close vicinity of the micromotor, including guidewires and stents, the design and manufacturing of an electromagnetic motor is quite critical. If the magnetic field is not fully contained in the motor, it may stop rotating or perform in an unpredictable fashion.

Ultrasonic motors do not suffer from this problem. In Tokyo, a new ultrasonic micromotor 1 mm in diameter and 3 mm in length has been built[42]. It can work in a liquid environment and is hollow, so that electronic connection wires for the transducer can pass through. The ultrasonic motor uses a wave guide in the shape of a helical coil as a stator. The coiled stator is placed inside or outside of the rotor and the stator is pressed to the rotor. The motor operates as a travelling wave type ultrasonic motor, a flexural wave propagates along the coiled acoustic wave guide. This so called "lamb wave" crawls like a caterpillar over the rotor. Since the stator is fixed this makes the rotor rotate. Two operational realizations of the motor are illustrated in Figure 3. In Figure 3a, the stator is placed outside the rotor, the diameter is 1 millimetre. In Figure 3b, the stator is placed inside the rotor. This version needs to miniaturized further since is has at present a diameter of 2 millimetres. The rotor of the first one is capable of rotating with a speed of approximately 500 - 2,000 r.p.m, the second one at 5000-8000 r.p.m., both according to the ultrasonic power delivered. Another feature of the motor is that the transducer to excite the Lamb wave and the driving part consisting of the rotor and the stator are separated. Since the former can be placed outside the body, the driving part can be made as small as 0.8 mm in diameter and 3mm in length. Although the concept works, the technology still needs to be transferred to a catheter.

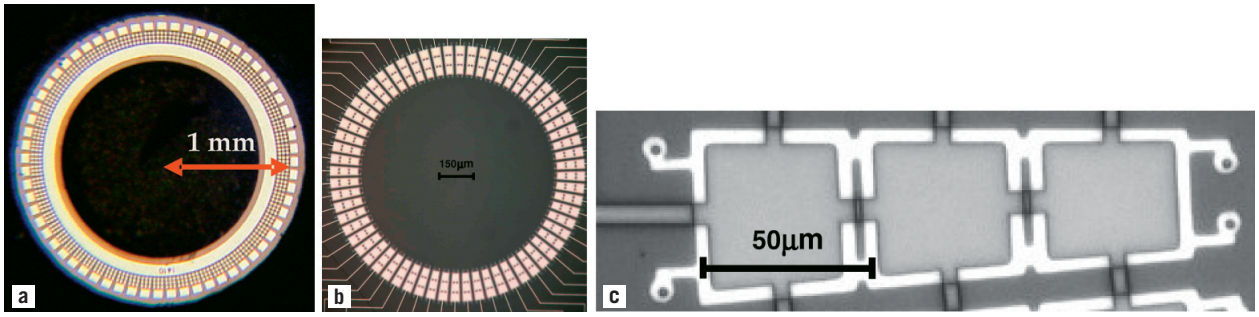

Figure 1. (a) Magnified view of the Stanford CMUT annular ring array. (b) Magnified view of the Georgia Tech CMUT annular ring array. (c) Further magnification of one element of the Georgia Tech array, each consists of f 3 rectangular cells connected in parallel.

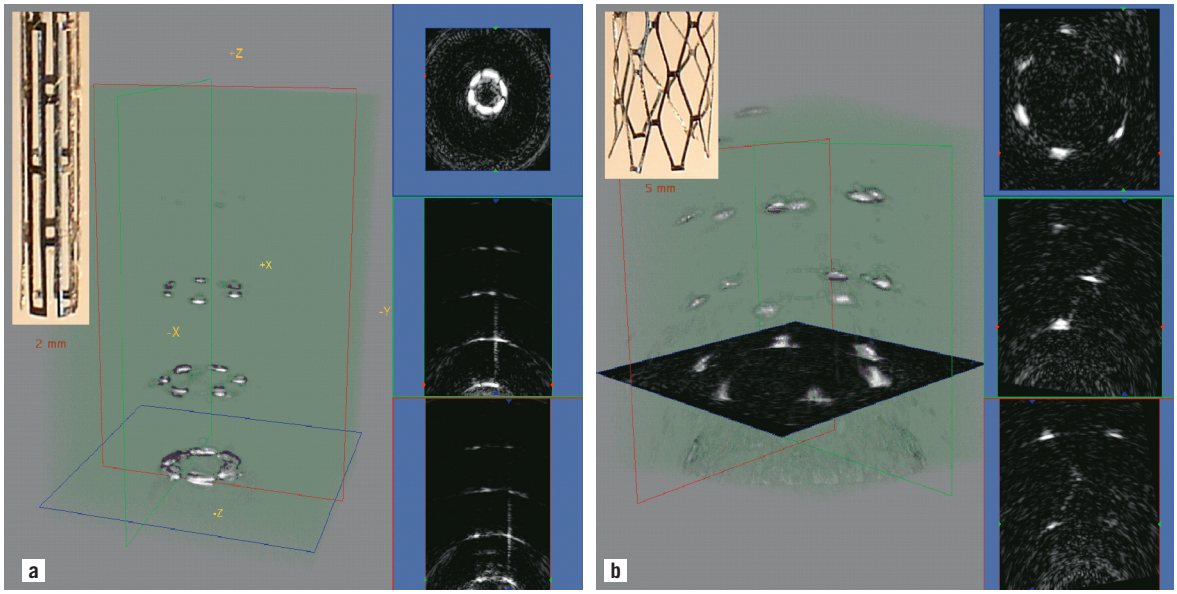

Figure 2. 3-D rendered ultrasound images and some cross-sections acquired with the Stanford array of (a) an undeployed Palmaz-Schatz stent; and (b) a deployed Palmaz-Schatz stent.

Harmonic IVUS

Since its introduction[43,44], Tissue Harmonic Imaging (THI) has increased the diagnostic value of conventional echocardiography. THI is a technique by which the received scattered ultrasound contains higher harmonics of the transmitted pulse due to non-linear sound propagation. THI enhances image quality through the combination of low harmonic content in the near field, a narrower beam, and reduced side lobe levels.

Although THI has been shown to increase image quality in medical ultrasound below 10 MHz, little work has been done to assess the benefits in IVUS applications. Initial studies showed the feasibility of THI at high frequencies for Ultrasound Biomicroscopy (UBM) and IVUS *in vitro*[45,46]. The reduction of stent imaging artifacts was shown when high frequency (20 - 40 MHz) THI was applied with a focused UBM transducer[47]. *In vivo* feasibility experiments of THI for an IVUS system using both a conventional and a custom-made mechanically-rotated IVUS catheter were described[48].

A prototype IVUS imaging system using a fast-rotating single element was constructed to do phantom experiments and perform *in vivo* imaging. To study the ability of a conventional IVUS catheter and a custom-made Harmonic IVUS catheter[49] to generate the required fundamental pressure to build up a detectable level of propagation harmonics, imaging experiments were performed. Data was acquired in fundamental 20 MHz (F20), harmonic 40 MHz (H40) mode, and for comparison purposes also in fundamental 40 MHz mode (F40). Harmonic images of cross-sections of an atherosclerotic aorta of a New Zealand White rabbit *in vivo* were formed by means of the Pulse Inversion (PI) technique. Signal-to-noise ratios (SNR) in H40 acquisitions were estimated *in vivo* for both catheters when driven by an F20 pulse with equal amplitude.

Cross-sectional images of the rabbit aorta *in vivo* were created using THI (Figure 4). The combined effect of amplifier saturation and reflections of the surrounding sheath, visible close to the transducer, is the least visible in H40 acquisition compared to both fundamental acquisitions. The latter emphasizes the advantage of reducing acoustic energy in the near field through the use of the harmonic beam. Recently, a transducer element (Figure 5) optimized for intravascular harmonic imaging, showing a frequency response

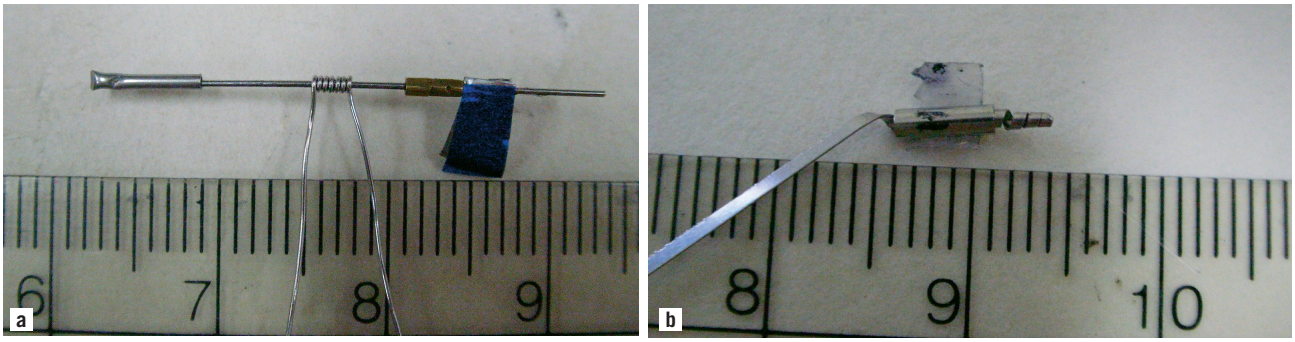

Figure 3. a. Ultrasound micromotor with an external stator. A flexural wave propagates along the coiled acoustic waveguide. This wave crawls like a caterpillar over the rotor, and makes it rotate. b. Ultrasound micromotor with an internal stator. (Scale is in cm)

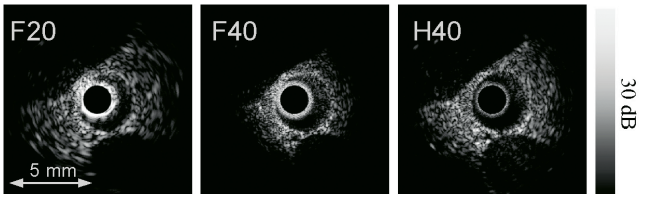

Figure 4. Cross-sections of an atherosclerotic rabbit aorta acquired in F20, F40 and H40 mode in vivo. These images are normalized with respect to the maximum signal level in the individual images.

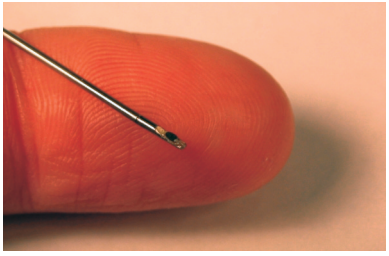

Figure 5a. The dual frequency transducer.

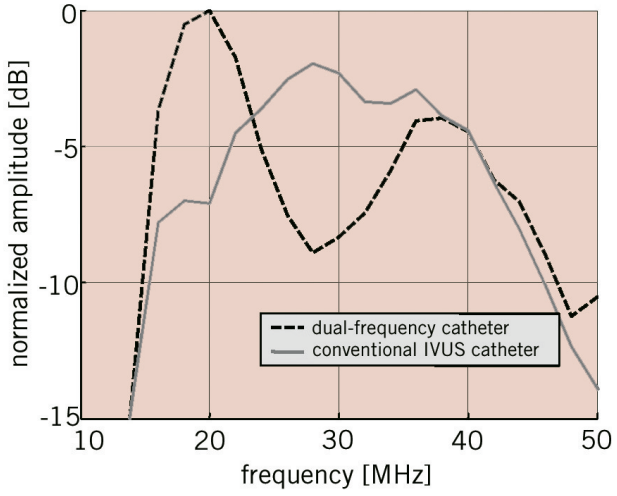

Figure 5b. One-way frequency responses of the dual-frequency catheter and a conventional IVUS catheter.

with two peaks around 20 and 40 MHz, has been designed, fabricated and characterized[49]. The main difference is an improved efficacy in transmit of 6 dB.

The *in vivo* imaging experiment resulted in a significant SNR improvement (>12 dB) in H40 mode of the custom-made catheter relative to the conventional catheter (Figure 6). However, careful interpretation is necessary since the aortas of only two different animals were imaged.

Incorporating optimised IVUS catheters for Harmonic Imaging indicates that instrumentation developments can improve harmonic IVUS imaging. Current studies investigate the feasibility of Harmonic IVUS with available clinical IVUS systems.

Contrast intravascular ultrasound

Microbubble contrast agents have been employed extensively at lower diagnostic ultrasound frequencies[50], but have seen little use in intravascular ultrasound. While microbubbles can in some circumstances be visualised through simple echogenicity enhancement, sensitive and specific detection of the agent is invariably

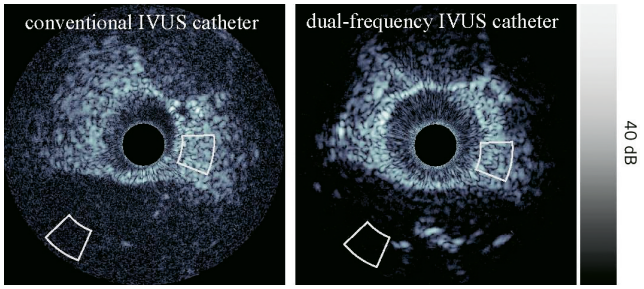

Figure 6. Cross-sections of rabbit aortas acquired in H40 mode with both a conventional and a dual-frequency IVUS catheter. Gray contours show the regions of interest for the SNR estimation.

achieved using more bubble-specific acoustic signatures. Two approaches employed successfully at lower frequencies are second harmonic imaging (listening at twice the ultrasound transmit frequency) and subharmonic imaging (listening at half the ultrasound transmit frequency). Using prototype instrumentation, it has recently been shown that microbubbles can be imaged in this manner with IVUS[51]. With these new approaches, two applications are possible: vasa vasorum imaging and molecular imaging.

Vasa vasorum imaging

It is well recognized that developing neovascular vasa vasorum is necessary for atherosclerotic plaque progression and that the microvascular status of lesions can be a marker for vulnerability to rupture[52,53]. At present, there are no established clinical tools capable of imaging coronary artery vasa vasorum[54]. Animal studies have been conducted to investigate the combination of microbubble contrast agents with prototype nonlinear IVUS systems to image vasa vasorum. In these experiments, the IVUS catheter was situated in a region of interest in an atherosclerotic rabbit aorta while contrast agent (Definity®, Bristol Myers Squibb) was released proximally in the form of a bolus through a delivery catheter. The agent was first detected within the main lumen, and then (after 5-10 second delay) within the adventitia surrounding the plaque (Figure 7). Quantification of the enhancement was statistically significant. In general, the spatial pattern of agent presence within the adventitia, and not the plaque itself, was consistent with the microvascular distribution revealed by histological sections taken in the vicinity of the imaging planes. These results indicate that contrast harmonic IVUS is capable of imaging features of vasa vasorum.

Molecular imaging

Targeted microbubble contrast agents used in conjunction with IVUS holds considerable potential for understanding the molecular status of atherosclerotic plaques, which may, in turn, impact plaque staging. A number of reports have indicated the feasibility of imaging microbubbles targeted to endothelial cell adhesion molecules[55] and fibrin[56]. These studies relied upon simple enhancement of echogenicity to determine the presence of microbubbles, and as such require the accumulation of considerable agent concentrations at target sites. The feasibility of bubble-specific imaging of targeted agent using a prototype nonlinear IVUS system was investigated[57]. The agent was an experimental biotinated, lipid encapsulated formulation comprised substantially of micron and submicron

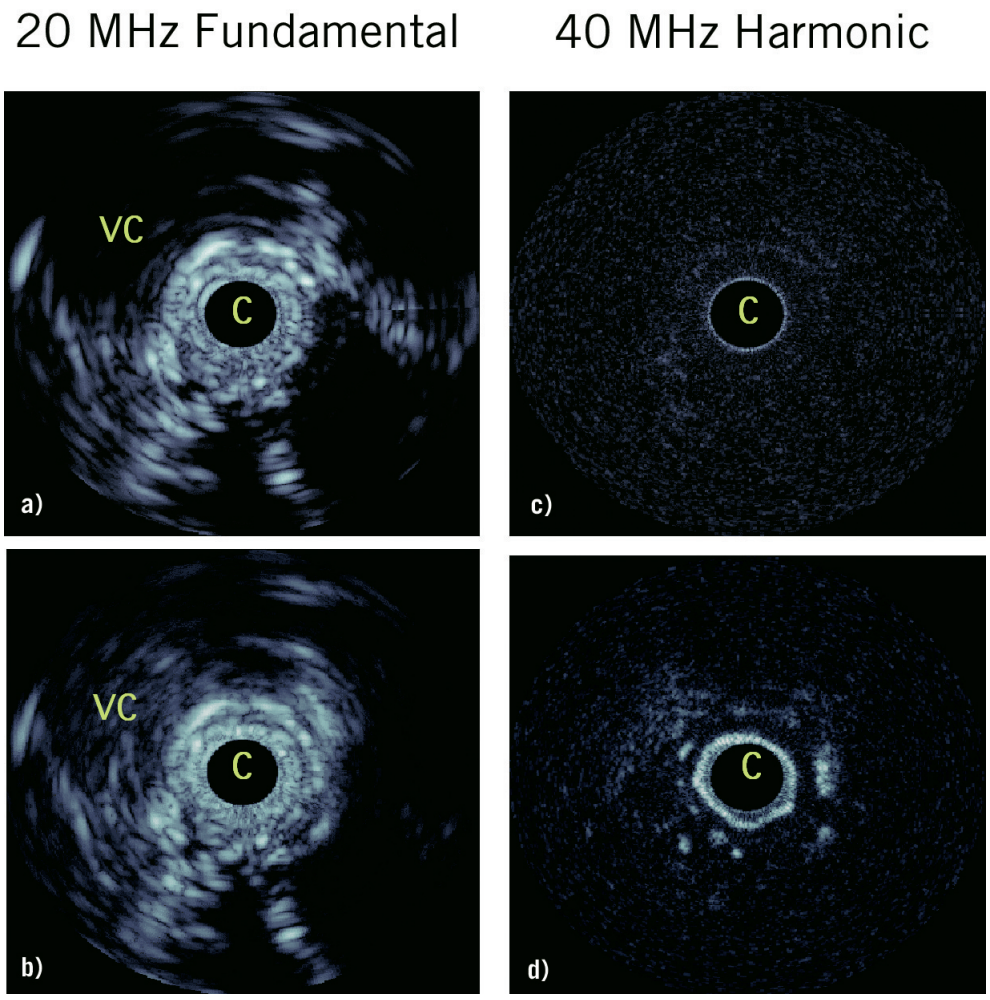

Figure 7. In vivo results in an atherosclerotic rabbit aorta using decanted Definity®. a) Fundamental mode prior to agent injection, where 'c' is the catheter, the vena cava is 'vc'. b) Fundamental mode 15 seconds post injection where changes in adventitial enhancement are not evident, except for in a region at 4 o'clock and within the vena cava. c) Harmonic mode prior to injection shows the tissue signals to be largely suppressed. d) 15 second post-injection harmonic mode shows significant adventitial enhancement, consistent with the detection of adventitial microvessels. Scale of images is 12 mm across. The dynamic range of the fundamental and harmonic images are 40 and 25 dB respectively.

sized bubbles (BG3039; Bracco Research, Geneva) targeted to an avidin coated agar substrate. Example images of tissue mimicking phantom coated with targeted contrast agents are shown in Figure 8. In fundamental (i.e. conventional 'linear' imaging) mode (Figure 8a), the agent is difficult to distinguish from background tissue signals. However, in second harmonic (not shown) and subharmonic (Figure 8b) modes the agent is clearly detected, with tissue signals suppressed below the noise floor. These results demonstrate the feasibility of harmonic imaging as a strategy for improving the sensitivity and specificity of targeted contrast agent detection at high ultrasound frequencies. Applicability of such molecular imaging approach *in vivo* still needs to be shown.

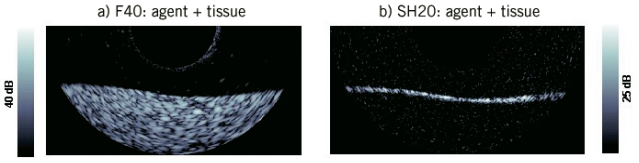

Figure 8. Agent targeted to tissue phantom in a) 40 MHz fundamental (F40) mode and b) in 20 MHz subharmonic (SH20) imaging modes. Image size 10 mm laterally, displaying half of rotational IVUS image.

Plaque characterization techniques

Structure and composition, rather than the degree of stenosis, are important characteristics of atherosclerotic plaques[58,59]. Identification of vulnerable plaques that consist of a lipid or necrotic core, covered by a thin fibrous cap, so called Thin Cap Fibro Atheromas (TCFA's) is particularly interesting, since the cap can rupture and if the necrotic core comes in touch with the blood it may create a thrombus that can occlude a vessel, causing an acute cardiovascular event. Hence, there is a need for a comprehensive imaging technique that can provide clinically relevant information both to detect and differentiate vulnerable plaques, and to determine the activity and the progression of the atherosclerotic lesion for appropriate management of the disease. Several techniques are under development for this task. Spectral analysis[60] of radiofrequency data is utilised in Virtual Histology[21], but there are several other approaches that may complement this technique, e.g. by

using self organizing maps[61]. The elastic properties of a plaque are explored by IVUS Palpography[30] and Elastography[62], but also this technique can be extended using Modulography or Thermal Strain Imaging[64]. Also combination with other imaging modalities like Photo-Acoustic Imaging[65] will likely increase sensitivity and specificity of the technique.

Intravascular photo-acoustic imaging

Catheter-based intravascular Photo-Acoustic (IVPA) imaging is being explored as a tool to identify and characterize the vulnerability of atherosclerotic plaques[66]. Integrated with intravascular ultrasound (IVUS) imaging[65], this combined technique will be capable of direct assessment of both functional and morphological properties of coronary atherosclerotic plaques, thus differentiating various types of plaques and efficiently guiding interventions with improved outcomes.

IVPA imaging is based on the detection of acoustic waves generated by laser pulses[66]. Specifically, the tissue is irradiated with short (3-10 ns) laser pulses with energy fluence (1-2 mJ/cm^2) far below the ablation threshold. As electromagnetic waves are differentially absorbed and tissue undergoes rapid thermoelastic expansion, broadband acoustic waves are generated within the irradiated volume.

Using an ultrasound detector (40-MHz IVUS catheter), these ultrasonic waves can be detected and spatially resolved to provide an image of internal tissue composition depicting the spatial distribution of optical absorbers. In IVPA imaging of arterial vessels, contrast is related to the optical absorption in intima, media, adventitia and atheromatous plaque[67]. In addition, photo-acoustic imaging has been integrated with IVUS. In this implementation, both IVPA and IVUS imaging systems utilize the same ultrasound sensor and associated receiver electronics allowing temporally consecutive, spatially concurrent ultrasonic and photo-acoustic imaging[65].

IVUS and IVPA images were obtained from an excised section of a normal rabbit artery using a 40-MHz IVUS catheter. (Figure 9) Each image covers a 6.67-mm diameter field of view with the IVUS catheter positioned at the centre. IVPA and IVUS images are spatially co-registered and show excellent correspondence. Both images illustrate the feasibility of obtaining reliable photo-acoustic signals from tissues and the ability to perform combined IVUS and IVPA imaging. The combined IVUS/IVPA image suggests that the area of functional interest can be delineated in the overall context of the vessel structure highlighting the importance and advantages of integration.

Combined IVPA and IVUS imaging can offer several advantages in imaging atherosclerotic plaques and may become an important clinical tool with sufficient sensitivity and specificity to guide coronary artery interventions. It is anticipated that IVPA/IVUS imaging may detect and differentiate different types of atherosclerotic plaques since both anatomical (morphology) and functional (activity) properties of the vessel are expected to change significantly with the presence of vulnerable plaque, and to a lesser extent with other atherosclerotic lesions. Imaging at high (few tenths of micrometers) spatial resolution should be possible in most cases since the IVPA/IVUS probe can be located inside the lumen and near the vessel wall and, therefore, high frequency ultrasound can be utilized. IVUS is routinely used in many cardiac catheterization laboratories to guide interventions, and therefore, all necessary pre-requisites for IVPA/IVUS imaging are readily available. Patients will not be subjected to any additional procedures, and the examination time will not increase to perform combined IVPA/IVUS imaging of the vessel. Both IVUS and IVPA are non-ionizing with no safety concerns. Finally, elasticity imaging or palpography[62] can also be integrated with IVUS/IVPA imaging to further enhance the clinical utility of IVUS[68,69].

IVUS RF data analysis for plaque classification using self-organizing maps

Spectral analysis of radiofrequency (RF) ultrasound signals may allow detailed assessment of plaque composition. The RF spectrum can be classified naturally using a self-organizing map (SOM) algorithm[61]. In this analysis method IVUS data are acquired with a commercially available IVUS system with a centre frequency of 40MHz. RF data are digitized and stored in a workstation using an A/D board with a sampling frequency of 500Msa/s and 8 bits resolution. After band pass filtering (15MHz-105MHz) and applying a 128 point Hamming window, the frequency spectrum is calculated for each position using an autoregressive (AR) model of order 15[70]. Optimized AR spectra are used to compute 18 spectral shape parameters for each ROI. These parameters are listed in Table 1.

The self-organizing map[71] is a neural network application used to classify these 18 parameters into seven categories which may correspond with catheter, shade, blood, fibrosis, calcium, lipid, media and others. In this study, the SOM classifier learned the spectral parameters for training. And then the SOM classifier indexed windowed areas of IVUS data based on these parameters. Finally, tis-

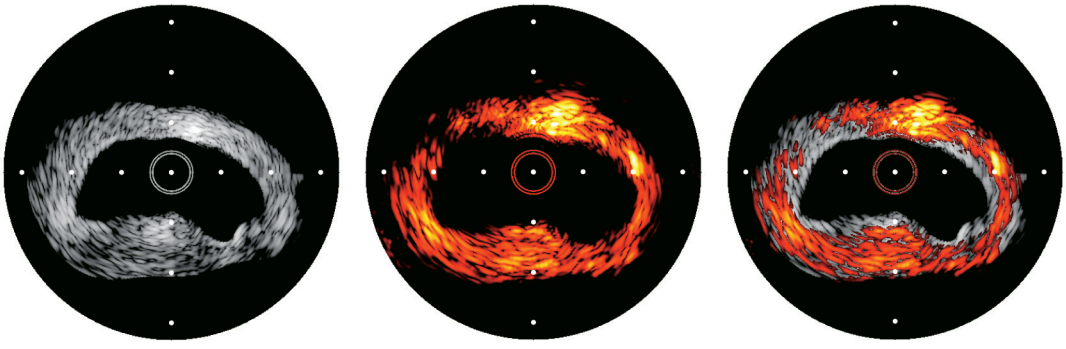

IVUS Image *IVPA Image* *Combined IVUS/IVPA image*

Figure 9. IVUS, photo-acoustic and combined image of a rabbit aorta.

Table 1. List of shape parameters classifying rf spectrum

1. Power of fundamental wave
2. Frequency of fundamental wave
3. Power of second harmonic wave
4. Frequency of second harmonic wave
5. Local minimum power between fundamental wave power and second harmonic wave power
6. Frequency of local minimum power
7. Maximum power
8. Frequency of maximum power
9. Slope from power at frequency 15MHz to fundamental wave power,
10. Corresponding y-intercept
11. Slope from fundamental wave power to local minimum power
12. Corresponding y-intercept
13. Slope from local minimum power to second harmonics power
14. Corresponding y-intercept
15. Slope from second harmonics power to 100MHz power
16. Corresponding y-intercept
17. Mean of integrated backscatter
18. ROI position at line.

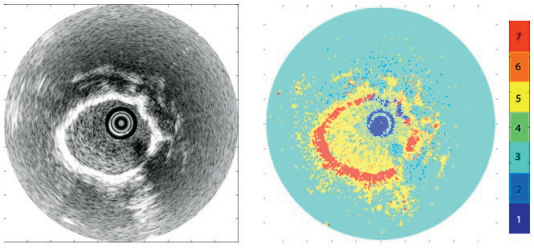

Figure 10. Conventional IVUS image (left) and color-coded image based on automatic classification by Self Organized Map (right).

sue maps were reconstructed on IVUS B-mode images based on the SOM. Table 2 gives sensitivities and specificities obtained from a limited initial data set (ref. proceedings). It is clear that extensive validation is still necessary.

Modulography: elasticity imaging of atherosclerotic coronary plaques

A new imaging technique called Modulography (concatenation of 'modulus' and 'graphy') has been developed to compute and visualize the elasticity distribution (i.e., the Young's modulus) of plaques

Table 2. Sensitivity and specificity of classified ROIs by the SOM (test data, table copied from Iwata *et al.*)

Kinds	Sensitivity	Specificity
Blood	100.0%	99.8%
Calcium	88.5%	99.8%
Catheter	99.2%	99.8%
Fibrous	88.3%	98.8%
Media	74.4%	96.7%
Others	92.8%	98.6%
Shade	88.3%	96.8%

in a so-called modulogram[63]. It directly shows the type and morphology of the main Thin Cap Fibro Atheroma (TCFA) components since the Young's modulus is a material parameter that is low for soft tissue and high for stiff tissue.

The procedure begins by computing a plaque's strain elastogram, [i.e., an image showing the deformation (strain) of the plaque caused by the pulsating blood pressure] using IVUS Elastography or Palpography[62,72,73]. Then, the plaque's modulogram is derived from the measured elastogram, as follows[74,75]: an optimization algorithm iteratively adjusts the shape and stiffness parameters of a TCFA computer-model (Figure 11), until the corresponding computer-model elastogram resembles the measured elastogram; the resulting morphology and stiffness values of the computer-model defines the modulogram. The computer-model's morphology parameters are the control-points of two deformable curves, one delineates the distal border of the lipid pool, the other the distal border of the cap; these components are assumed homogeneous and their stiffness is characterized by a YM. The inner and outer boundaries of the computer-model are contour-detected from the plaque's IVUS echogram.

Modulography successfully derived modulograms from simulated and measured elastograms of TCFA plaques. The modulograms clearly showed the morphology and stiffness of the cap and lipid pool; this information is generally not directly identifiable from the echogram or elastogram (Figure 12).

The computer-model's TCFA geometry was essential *a priori* information that allowed a stable derivation of the modulogram. However, plaques can also be heterogeneous, consisting of multiple regions of soft and stiff tissue. Therefore, we are currently generalizing Modulography, so that it works for arbitrary plaques[76]. To advance Modulography into the clinic a thorough validation study is required, as well as a pre-processing method for fully automatic assessment of proper elastograms i*n vivo*[77]. As an addition to IVUS Elastography and Palpography, Modulography has strong potential

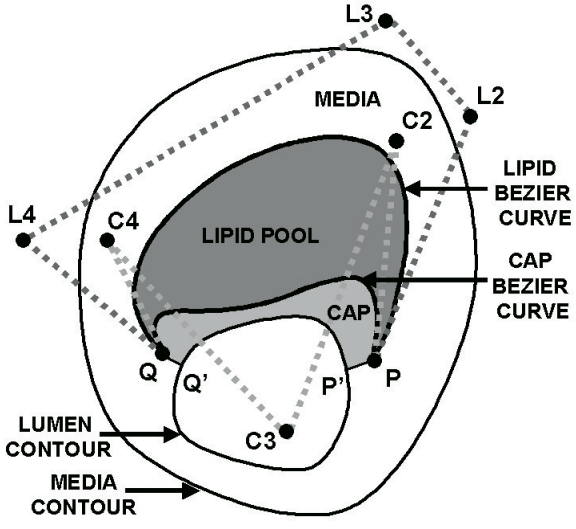

Figure 11. Computer-model of a thin-cap fibroatheroma plaque. The shape of the lipid and cap deformable Bézier curves are determined by the spatial locations of their control points. In this example there are 5 control points used for the lipid curve namely P, L2, L3, L4 and Q, and also 5 for the cap curve, namely P, C2, C3, C4 and Q.

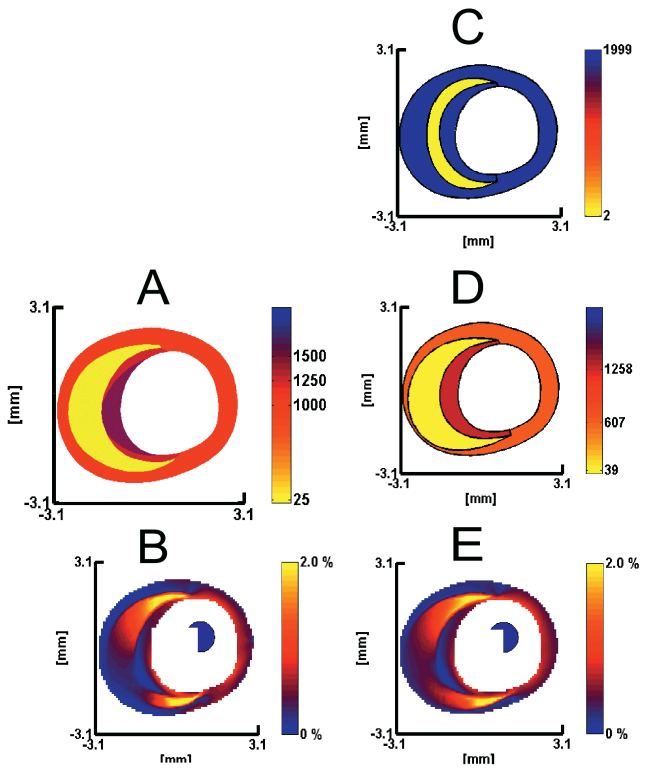

Figure 12. Modulography using a simulated strain elastogram of a thin-cap fibroatheroma plaque; its geometry and elastic material distribution was determined from tracing human coronary plaque histology. (a) Modulogram of the traced plaque; the Young's moduli of its plaque components are ELIPID=25, EMEDIA=1000 and ECAP=1250 at center / 1500 at side regions. (b) Simulated elastogram computed from a. (c) Default modulogram at the start of the optimization process. (d) Final modulogram at the end of the optimization process, derived from b. (e) Strain elastogram computed from d. Notice the resemblance between elastograms b and e, as well as the similarity between modulograms a and d. Young's moduli are in kPa and the intraluminal pressure difference is 20 mmHg. The range of each Young's modulus colour bar is (0-2000) kPa.

to become an all-in-one IVUS-based tissue characterization tool for detecting coronary plaques[73], for assessing information related to their proneness to rupture[30], and for imaging their elastic material composition, all *in vivo*.

High resolution thermal strain imaging

It is well known that lipids have a negative temperature dependence of the sound speed, whereas water-based tissues have positive temperature dependence. Controlled local temperature modulation can be used to image the spatial distribution of temporal strain produced by changes in sound speed. The opposite sign of the two different tissue types creates the contrast required for resolving the lipid-laden pool within a vulnerable plaque from surrounding water-based arterial wall. High resolution Thermal Strain Imaging (TSI) using an ultrasound (US) microscope was applied to excised porcine tissues[63,78]. Samples were placed in a temperature controlled water chamber and scanned transversely and longitudinally using a custom high resolution microscope.

An illustration of the experimental system is presented in Figure 13. Phase sensitive, correlation based speckle tracking was applied to map the spatial distribution of temporal strain across the sample. TSI

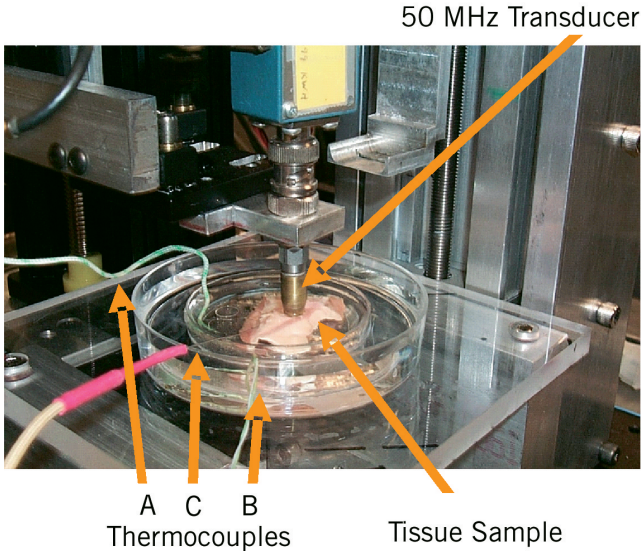

Figure 13. Experimental Set-up: Ultrasound Microscope. The coronary artery sample is held by a clip mounted at the bottom of the inner Petri dish. The outer Petri dish serves as a container for warm water to control temperature. Thermocouples monitor the temperature in the Petri dishes and inside the tissue. The single element transducer is fastened to the positioning slider driven by a stepping motor.

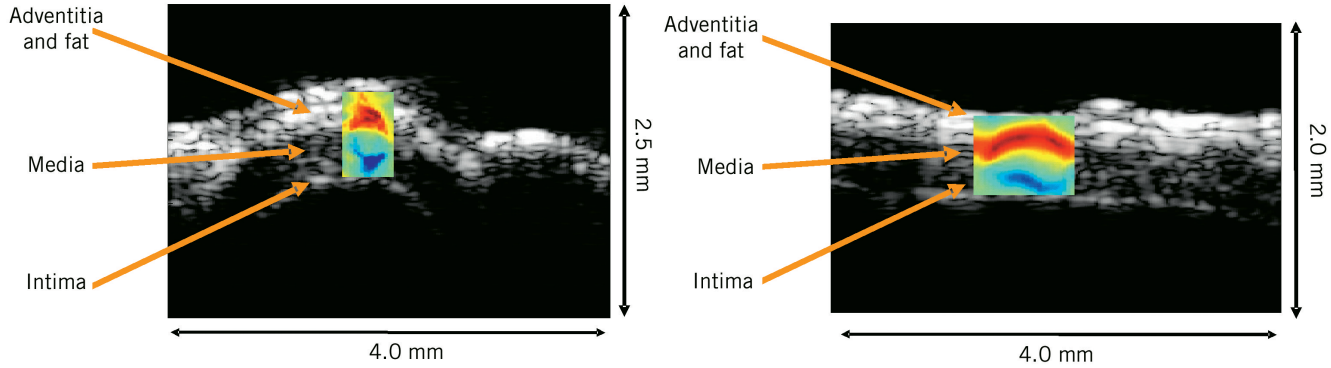

Figure 14. TSI of porcine coronary artery overlaid on the B-Scan. The top is the transverse scan and the bottom is the longitudinal scan. The dynamic range of the TSI is +/- 0.5 % over 4-5oC change in temperature. TSI images correlate well with B-Scans.

differentiated fatty tissue from the water based arterial wall and muscle with high contrast and a spatial resolution of 60 microns for a 50 MHz transducer. Both transverse and longitudinal TSI images compare well with B-Scans of arterial wall structures, including intima, media, adventitia and overlying fatty tissue, as illustrated in Figure 14. High resolution TSI images of coronary artery compare well with B-Scans of the arterial wall structure, including intima, media, adventitia and fatty tissue. This *ex-vivo* result demonstrates the feasibility of TSI for atherosclerotic plaque detection and monitoring at high resolution. A major obstacle for *in-vivo* application is tissue motion, including respiratory and cardiac motion. Motion compensation using spatial interpolation and linear least squares fitting can minimize the adverse effect of tissue motion[79].

Conclusion

In this paper several new intravascular ultrasound technologies are discussed that have been presented at the 2005 IEEE Ultrasonics symposium. All have high potential, but none is clinically available at present. Still it is clear that the development of IVUS technology is focus of attention in many research laboratories, which will result in the evolution of many high impact applications. Possibilities that are presently beyond the horizon will come within reach in the foreseeable future.

References

1. Y. Saijo, A.F.W. van der Steen, Vascular Ultrasound. Tokyo: Springer, 2003.

2. C.T. Lancee, N. Bom. Apparatus for ultrasonically examining a hollow organ, UK patent 1402192, US patent 3,827,115. 1972.

3. N. Bom, C.T. Lancee, F.C. van Egmond. An ultrasonic intracardiac scanner. *Ultrasonics,* vol. 10, pp. 72-76, 1972.

4. W.J. Gussenhoven, C.E. Essed, P. Frietman, F. Mastik, C.T. Lancee, C.J. Slager, P.W. Serruys, P. Gerritsen, H. Pieterman, N. Bom. Intravascular echographic assessment of vessel wall characteristics: A correlation with histology. *Intravascular ultrasound,* N. Bom and J. Roelandt, Eds. Dordrecht: Kluwer, 1989, pp. 105-115.

5. P.G. Yock, D.T. Linker, N.W. White, M.H. Rowe, M.R. Selmon, G.C. Robertson, T. Hinohara, J.B. Simpson. Clinical applications of intravascular ultrasound imaging in atheroma. In Intravascular ultrasound, N. Bom and J. Roelandt, Eds. Dordrecht: Kluwer, 1989, pp. 117-124.

6. C. von Birgelen, W. Li, N. Bom, P.W. Serruys. Quantitative three-dimensional intravascular ultrasound. Semin Interv Cardiol, vol. 2, pp. 25-32, 1997.

7. C. von Birgelen, M. Hartmann, G.S. Mintz, D. Baumgart, A. Schmermund, R. Erbel. Relation between progression and regression of atherosclerotic left main coronary artery disease and serum cholesterol levels as assessed with serial long-term (> or =12 months) follow-up intravascular ultrasound. *Circulation,* vol. 108, pp. 2757-62, 2003.

8. S.E. Nissen, E.M. Tuzcu, P. Schoenhagen, B.G. Brown, P. Ganz, R.A. Vogel, T. Crowe, G. Howard, C.J. Cooper, B. Brodie, C.L. Grines, A.N. DeMaria. Effect of intensive compared with moderate lipid-lowering therapy on progression of coronary atherosclerosis: a randomized controlled trial. *JAMA,* vol. 291, pp. 1071-80, 2004.

9. P.W. Serruys, M. Degertekin, K. Tanabe, A. Abizaid, J.E. Sousa, A. Colombo, G. Guagliumi, W. Wijns, W.K. Lindeboom, J. Ligthart, P.J. de Feyter, M.C. Morice. Intravascular ultrasound findings in the multicenter, randomized, double-blind RAVEL (RAndomized study with the sirolimus-eluting VElocity balloon-expandable stent in the treatment of patients with de novo native coronary artery Lesions) trial. *Circulation,* vol. 106, pp. 798-803, 2002.

10. S.G. Carlier, J.P. Marijnissen, V.L. Coen, W.J. van der Giessen, M. Sabate, J. Ligthart, A. den Boer, I.E. Cespedes, W. Li, A.F. van der Steen, P.C. Levendag, P.W. Serruys. Guidance of intracoronary radiation therapy based on dose-volume histograms derived from quantitative intravascular ultrasound. *IEEE Trans Med Imaging,* vol. 17, pp. 772-8, 1998.

11. C.J. Slager, J.J. Wentzel, F.J. Gijsen, J.C. Schuurbiers, A.C. van der Wal, A.F. van der Steen, P.W. Serruys. The role of shear stress in the generation of rupture-prone vulnerable plaques. *Nat Clin Pract Cardiovasc Med,* vol. 2, pp. 401-7, 2005.

12. R. Krams, J.J. Wentzel, J.A. Oomen, R. Vinke, J.C. Schuurbiers, P.J. de Feyter, P.W. Serruys, C.J. Slager. Evaluation of endothelial shear stress and 3D geometry as factors determining the development of atherosclerosis and remodeling in human coronary arteries in vivo. Combining 3D reconstruction from angiography and IVUS (ANGUS) with computational fluid dynamics. *Arterioscler Thromb Vasc Biol,* vol. 17, pp. 2061-5, 1997.

13. C.L. Feldman, A.U. Coskun, Y. Yeghiazarians, S. Kinlay, A. Wahle, M.E. Olszewski, J.D. Rossen, M. Sonka, J.J. Popma, J. Orav, R.E. Kuntz, P.H. Stone. Remodeling characteristics of minimally diseased coronary arteries are consistent along the length of the artery. *Am J Cardiol,* vol. 97, pp. 13-6, 2006.

14. M. O'Donnell, M.J. Eberle, D.N. Stephens, J.L. Litzza, B.M. Shapo, J.R. Crowe, C.D. Choi, J.J. Chen, D.M. W. Muller, J.A. Kovach, R.L. Lederman, R.C. Ziegenbein, C.C. Wu, K. San Vincente, D. Bleam. Catheter arrays: can intravascular ultrasound make a difference in managing coronary artery disease. *IEEE Ultrasonics Symposium,* 1447-1456 1997.

15. A.F.W. van der Steen, E.I. Cespédes, C.L. de Korte, S.G. Carlier, W. Li, F. Mastik, C.T. Lancée, J. Borsboom, F. Lupotti, R. Krams, P.W. Serruys, N. Bom. Novel developments in intravascular imaging. *IEEE Ultrasonics Symposium,* 1733-1742 1998.

16. M. O'Donnell. Phased array beam forming from a circular array: applications to imaging of coronary arteries. *IEEE UltrasonicsI Symposium,* pp. 637-640, 1991.

17. U. Demirci, A.S. Ergun, O. Oralkan, M. Karaman, B.T. Khuri-Yakub. Forward-viewing CMUT arrays for medical Imaging. *IEEE Transactions on Ultrasonics Ferroelectrics and Frequency Control,* vol. 51, pp. 887-895, 2004.

18. Y. Wang, D.N. Stephens, M. O'Donnell. Optimizing the beam pattern of a forward-viewing ring-annular ultrasound array for intravascular imaging. *IEEE Transactions on Ultrasonics Ferroelectrics and Frequency Control,* vol. 49, pp. 1652-1664, 2002.

19. J.R. Crowe, B.M. Shapo, D.N. Stephens, D. Bleam, M.J. Eberle, C.C. Wu, D.M.W. Muller, J.A. Kovatch, R.L. Lederman, M. O'Donnell. Coronary artery flow imaging with an Intraluminal array. *IEEE Ultrasonics Symposium,* pp. 1481-1484, 1996.

20. E.I. Cespédes, W. Li, F. Mastik, A.F.W. van der Steen, S.G. Carlier, R.H. van Bremen, M. Eberle, N. Bom. Intravascular Power Flow Imaging: Theory and potentials for planimetry. *IEEE Ultrasonics Symposium,* pp. 1273-1276, 1997.

21. W. Li, A.F. van der Steen, C.T. Lancee, I. Cespedes, N. Bom. Blood flow imaging and volume flow quantitation with intravascular ultrasound. *Ultrasound Med Biol,* vol. 24, pp. 203-14, 1998.

22. J.R. Crowe, M. O'Donnell. .Quantitative blood speed imaging with intravascular ultrasound. *IEEE Trans Ultrason Ferroelectr Freq Control,* vol. 48, pp. 477-87, 2001.

23. S.G. Carlier, W. Li, I. Cespedes, A.F. van der Steen, J.N. Hamburger, N. Bom, P. W. Serruys. Images in cardiovascular medicine. Simultaneous morphological and functional assessment of a renal artery stent intervention with intravascular ultrasound. *Circulation,* vol. 97, pp. 2575-6, 1998.

24. S.L. Bridal, P. Fornes, P. Bruneval, G. Berger. Parametric (integrated backscatter and attenuation) images constructed using backscattered radio frequency signals (25-56 MHz) from human aortae in vitro. *Ultrasound Med Biol,* vol. 23, pp. 215-29, 1997.

25. T. Spencer, M.P. Ramo, D.M. Salter, T. Anderson, P.P. Kearney, G.R. Sutherland, K.A. Fox, W.N. McDicken. Characterisation of atherosclerotic plaque by spectral analysis of intravascular ultrasound: an in vitro methodology. *Ultrasound Med Biol,* vol. 23, pp. 191-203, 1997.

26. A. Nair, B. D. Kuban, E. M. Tuzcu, P. Schoenhagen, S.E. Nissen, D.G. Vince, Coronary plaque classification with intravascular ultrasound radiofrequency data analysis. *Circulation,* vol. 106, pp. 2200-2206, 2002.

27. S.A. Wickline, J.G. Miller, D. Recchia, A.M. Sharkey, S.L. Bridal, D.H. Christ. Beyond intravascular imaging: Quantitative ultrasonic tissue characterization of vascular pathology. *IEEE Ultrasonics Symposium,* pp. 1589-1598, 1994.

28. L.K. Ryan, F.S. Foster. Ultrasonic measurement of differential displacement and strain in a vascular model. *Ultrason Imaging,* vol. 19, pp. 19-38, 1997.

29. C.L. de Korte, E.I. Cespedes, A.F. van der Steen, G. Pasterkamp, N. Bom. Intravascular ultrasound elastography: assessment and imaging of elastic properties of diseased arteries and vulnerable plaque. *Eur J Ultrasound,* vol. 7, pp. 219-24, 1998.

30. J.A. Schaar, C.L. De Korte, F. Mastik, C. Strijder, G. Pasterkamp, E. Boersma, P.W. Serruys, A.F.W. Van Der Steen. Characterizing vulnerable plaque features with intravascular elastography. *Circulation,* vol. 108, pp. 2636-41, 2003.

31. Y. Saijo, S. Tanaka, N. Owada, Y. Akino, S. Nitta. Tissue velocity imaging of coronary artery by rotating-type intravascular ultrasound. *Ultrasonics,* vol. 42, pp. 753-757, 2004.

32. B.M. Shapo, J.R. Crowe, R. Erkamp, S.Y. Emelianov, M.J. Eberle, M. O'Donnell. Strain imaging of coronary arteries with intraluminal ultrasound: experiments on an inhomogeneous phantom. *Ultrason Imaging,* vol. 18, pp. 173-91, 1996.

33. O. Oralkan, A.S. Ergun, J.A. Johnson, M. Karaman, U. Demirci, K. Kaviani, T.H. Lee, B.T. Khuri-Yakub. Capacitive micromachined ultrasonic transducers: Next-generation arrays for acoustic imaging? *IEEE Transactions on Ultrasonics Ferroelectrics and Frequency Control,* vol. 49, pp. 1596-1610, 2002.

34. F.L. Degertekin, R.O. Guldiken, M. Karaman. Micromachined Capacitive Transducer Arrays for Intravascular Ultrasound Imaging, presented at SPIE Symposium on MOEMS Display and Imaging Systems, 2005.

35. D.T. Yeh, O. Oralkan, I.O. Wygant, M. O'Donnell, B.T. Khuri-Yakub. 3-D Ultrasound Imaging Using Forward Viewing CMUT Ring Arrays for Intravascular and Intracardiac Applications. *IEEE Ultrasonics Symposium,* pp. 783-786, 2005.

36. F.L. Degertekin, M. Karaman, R.O. Guldiken. Forward-Looking IVUS Imaging Using an Annular-Ring CMUT Array. *IEEE Ultrasonics Symposium,* pp. 129-132, 2005.

37. J. Knight, J. McLean, F.L. Degertekin. Low temperature fabrication of immersion capacitive micromachined ultrasonic transducers on silicon and dielectric substrates. *IEEE Transactions on Ultrasonics Ferroelectrics and Frequency Control,* vol. 51, pp. 1324-1333, 2004.

38. F.L. Degertekin, R.O. Guldiken, M. Karaman. Annular-ring CMUT arrays for forward-looking IVUS: transducer characterization and imaging. *IEEE Trans Ultrason Ferroelectr Freq Control,* vol. 53, pp. 474-482, 2006.

39. H. ten Hoff, A. Korbijn, T.H. Smith, J.F. Klinkhamer, N. Bom. Imaging artifacts in mechanically driven ultrasound catheters. *Int J Card Imaging,* vol. 4, pp. 195-9, 1989.

40. C.T. Lancee, N. Bom, J. Roelandt. Future directions in intravascular ultrasound: from micro-motors to imaging guidewire systems. *Echocardiography,* vol. 12, pp. 275-81, 1995.

41. N. Bom, S.G. Carlier, A.F. van der Steen, C.T. Lancee. Intravascular scanners. *Ultrasound Med Biol,* vol. 26 Suppl 1, pp. S6-9, 2000.

42. T. Moriya, Y. Akano, Y. Furukawa, A. Nakajima. Development of a Miniature Ultrasonic Motor Using a Helical Coil as a Stator. *IEEE Ultrasonics Symposium,* pp. 1546-1549, 2005.

43. M.A. Averkiou, D.N. Roundhill, J.E. Powers. A new imaging technique based on the nonlinear properties of tissues. *IEEE Ultrasonics Symposium,* pp. 1561-1566, 1997.

44. B. Ward, A.C. Baker, V.F. Humphrey. Nonlinear propagation applied to the improvement of lateral resolution in medical ultrasound scanners, presented at World Congress on Ultrasonics, 1995.

45. E.W. Cherin, J.K. Poulsen, A.F. W. van der Steen, P. Lum, F.S. Foster. Experimental characterization of fundamental and second harmonic beams for a high-frequency ultrasound transducer. *Ultrasound Med Biol,* vol. 28, pp. 635-46, 2002.

46. A.F.W. van der Steen, J.K. Poulsen, E. Cherin, F.S. Foster. Harmonic imaging at high frequencies for IVUS. *IEEE Ultrasonics Symposium,* pp. 1537-1540, 1999.

47. M.E. Frijlink, D.E. Goertz, A.F.W. van der Steen. Reduction of stent artifacts using high-frequency harmonic ultrasound imaging. *Ultrasound Med Biol,* vol. 31, pp. 1335-1342, 2005.

48. M.E. Frijlink, D.E. Goertz, H.J. Vos, E. Droog, G. Blacquière, A. Gisolf, A.F.W. van der Steen. Harmonic Intravascular Ultrasound Imaging with a dual-frequency catheter. *IEEE Ultrasonics Symposium,* pp. 241-244, 2005.

49. H.J. Vos, M.E. Frijlink, E. Droog, D.E. Goertz, G. Blacquière, A. Gisolf, N. de Jong, A.F.W. van der Steen. Transducer for Harmonic Intravascular Ultrasound Imaging. *IEEE Trans Ultrason Ferroelectr Freq Control,* vol. 52, pp. 2418-2422, 2005.

50. B.B. Goldberg, Ultrasound contrast agents: Basic principles and clinical applications in echocardiography, vol. Second edition. London: Martin Dunitz, 2001.

51. D.E. Goertz, M.E. Frijlink, N. de Jong, A.F.W. van der Steen. Nonlinear intravascular ultrasound contrast imaging. *Ultrasound Med Biol,* in press.

52. K.S. Moulton. Plaque angiogenesis: its functions and regulation. *Cold Spring Harb Symp Quant Biol,* vol. 67, pp. 471-82, 2002.

53. P.R. Moreno, K.R. Purushothaman, V. Fuster, D. Echeverri, H. Truszczynska, S.K. Sharma, J.J. Badimon, W.N. O'Connor. Plaque neovascularization is increased in ruptured atherosclerotic lesions of human aorta: implications for plaque vulnerability. *Circulation,* vol. 110, pp. 2032-8, 2004.

54. D.E. Goertz, M.E. Frijlink, D. Tempel, R. Krams, P. W. Serruys, F. ten Cate, J.A. Schaar, N. de Jong, A.F.W. van der Steen. Contrast harmonic intravascular ultrasound: a feasibility study for vasa vasorum imaging. *Investigative Radiology,* submitted.

55. F.S. Villanueva, R.J. Jankowski, S. Klibanov, M.L. Pina, S.M. Alber, S.C. Watkins, G.H. Brandenburger, W.R. Wagner. Microbubbles targeted to intercellular adhesion molecule-1 bind to activated coronary artery endothelial cells. *Circulation,* vol. 98, pp. 1-5, 1998.

56. S.M. Demos, H. Alkan-Onyuksel, B.J. Kane, K. Ramani, A. Nagaraj, R. Greene, M. Klegerman, D.D. McPherson. In vivo targeting of acoustically reflective liposomes for intravascular and transvascular ultrasonic enhancement. *J Am Coll Cardiol,* vol. 33, pp. 867-75, 1999.

57. D.E. Goertz, J.E.T. van Wamel, M.E. Frijlink, N. de Jong, A.F.W. van der Steen. Nonlinear Imaging of Targeted Microbubbles with Intravascular Ultrasound. *IEEE Ultrasonics Symposium,* pp. 2003-2006, 2005.

58. J.A. Schaar, J.E. Muller, E. Falk, R. Virmani, V. Fuster, P.W. Serruys, A. Colombo, C. Stefanadis, S. Ward Casscells, P.R. Moreno, A. Maseri, A.F. van der Steen. Terminology for high-risk and vulnerable coronary artery plaques. Report of a meeting on the vulnerable plaque, June 17 and 18, 2003, Santorini, Greece. *Eur Heart J,* vol. 25, pp. 1077-82, 2004.

59. M. Naghavi, P. Libby, E. Falk, S.W. Casscells, S. Litovsky, J. Rumberger, J.J. Badimon, C. Stefanadis, P. Moreno, G. Pasterkamp, Z. Fayad, P.H. Stone, S. Waxman, P. Raggi, M. Madjid, A. Zarrabi, A. Burke, C. Yuan, P.J. Fitzgerald, D.S. Siscovick, C.L. de Korte, M. Aikawa, K.E. Juhani Airaksinen, G. Assmann, C.R. Becker, J.H. Chesebro, A. Farb, Z.S. Galis, C. Jackson, I.K. Jang, W. Koenig, R.A. Lodder, K. March, J. Demirovic, M. Navab, S.G. Priori, M.D. Rekhter, R. Bahr, S.M. Grundy, R. Mehran, A. Colombo, E. Boerwinkle, C. Ballantyne, W. Insull, Jr., R.S. Schwartz, R. Vogel, P.W. Serruys, G.K. Hansson, D.P. Faxon, S. Kaul, H. Drexler, P. Greenland, J.E. Muller, R. Virmani, P.M. Ridker, D.P. Zipes, P.K. Shah, J.T. Willerson. From vulnerable plaque to vulnerable patient: a call for new definitions and risk assessment strategies: Part I. *Circulation,* vol. 108, pp. 1664-72, 2003.

60. Z.A. Fayad, V. Fuster. Clinical imaging of the high-risk or vulnerable atherosclerotic plaque. *Circ Res,* vol. 89, pp. 305-16, 2001.

61. T. Iwamoto, A. Tanaka, Y. Saijo, M. Yoshizawa. Coronary Plaque Classification through Intravascular Ultrasound Radiofrequency Data Analysis Using Self-organizing Map. *IEEE Ultrasonics Symposium,* pp. 2054-2057, 2005.

62. C.L. de Korte, M.J. Sierevogel, F. Mastik, C. Strijder, J.A. Schaar, E. Velema, G. Pasterkamp, P.W. Serruys, A.F.W. van der Steen. Identification of atherosclerotic plaque components with intravascular ultrasound elastography in vivo: a Yucatan pig study. *Circulation,* vol. 105, pp. 1627-1630, 2002.

63. R.A. Baldewsing, F. Mastik, J.A. Schaar, A.F.W. van der Steen. Young's Modulus Reconstruction and Delineation of Vulnerable Atherosclerotic Plaque Components. *IEEE Ultrasonics Symposium,* pp. 249-252, 2005.

64. K. Kim, R. Witte, M. O'Donnell. Arterial Lipid Characterization by High Resolution TSI. *IEEE Ultrasonics Symposium,* pp. 137-140, 2005.

65. S. Sethuraman, S.R. Aglyamov, J.H. Amirian, R.W. Smalling, S.Y. Emelianov. Development of a combined intravascular ultrasound and photoacoustic imaging system, presented at Proceedings of the 2006 SPIE Photonics West Symposium: Photons Plus Ultrasound: Imaging and Sensing, 2006.

66. S. Sethuraman, S.R. Aglyamov, J.H. Amirian, R.W. Smalling, S.Y. Emelianov. Intravascular photoacoustic imaging to detect and differentiate atherosclerotic plaques. *IEEE Ultrasonics Symposium,* pp. 133-136, 2005.

67. P.C. Beard, T.N. Mills. Characterization of post mortem arterial tissue using time-resolved photoacoustic spectroscopy at 436, 461 and 532 nm. *Phys Med Biol,* vol. 42, pp. 177-98, 1997.

68. S. Sethuraman, S.R. Aglyamov, J.H. Amirian, R.W. Smalling, S.Y. Emelianov. An integrated ultrasound-based intravascular imaging of atherosclerosis, presented at Proceedings of the Fourth International Conference on the Ultrasonic Measurement and Imaging of Tissue Elasticity, 2005.

69. S.Y. Emelianov, S.R. Aglyamov, J. Shah, S. Sethuraman, W.G. Scott, R. Schmitt, M. Motamedi, A. Karpiouk, A. Oraevsky. Combined ultrasound, optoacoustic and elasticity imaging, presented at Proceedings of the 2004 SPIE Photonics West Symposium: Photons Plus Ultrasound: Imaging and Sensing, 2004.

70. T. Baldeweck, P. Laugier, A. Herment, G. Berger. Application of Autoregressive Spectral-Analysis for Ultrasound Attenuation Estimation - Interest in Highly Attenuating Medium. *IEEE Transactions on Ultrasonics Ferroelectrics and Frequency Control,* vol. 42, pp. 99-110, 1995.

71. T. Kohonen, *Self-Organizing Maps,* vol. 30, 3rd ed. Berlin, Heidelberg, New York: Springer, 2001.

72. M. Doyley, F. Mastik, C.L. de Korte, S. Carlier, E. Cespedes, P. Serruys, N. Bom, A.F.W. van der Steen. Advancing intravascular ultrasonic palpation towards clinical applications. *Ultrasound Med Biol,* vol. 27, pp. 1471-1480, 2001.

73. J.A. Schaar, E. Regar, F. Mastik, E.P. McFadden, F. Saia, C. Disco, C.L. de Korte, P.J. de Feyter, A.F.W. van der Steen, P.W. Serruys. Incidence of vulnerable plaque patterns in humans: assessment with three-dimensional intravascular palpography and correlation with clinical presentation. *Circulation,* vol. 109, pp. 2716-2719, 2004.

74. R.A. Baldewsing, F. Mastik, J.A. Schaar, P.W. Serruys, A.F.W. van der Steen. Young's modulus reconstruction of vulnerable atherosclerotic plaque components using deformable curves. *Ultrasound in Med Biol,* vol. 32, pp. 201-210, 2005.

75. R.A. Baldewsing, J.A. Schaar, F. Mastik, C.W.J. Oomens, A.F.W. van der Steen. Assessment of vulnerable plaque composition by matching the deformation of a parametric plaque model to measured plaque deformation. *IEEE Trans Med Imaging,* vol. 24, pp. 514-528, 2005.

76. R.A. Baldewsing, F. Mastik, J.A. Schaar, A.F.W. van der Steen. A compounding method for reconstructing the heterogeneous Young's modulus distribution of atherosclerotic plaques from their radial strain. Proceedings of the Fourth International Conference on the Ultrasonic Measurement and Imaging of Tissue Elasticity, pp. 68, 2005.

77. K.Y.E. Leung, R.A. Baldewsing, F. Mastik, J.A. Schaar, A. Gisolf, A.F.W. van der Steen. Motion Compensation for Intravascular Ultrasound Palpography. *IEEE Trans Ultrason Ferroelectr Freq Control,* vol. 53 in press, 2005.

78. Y. Shi, R.S. Witte, M. O'Donnell. Identification of vulnerable atherosclerotic plaque using IVUS-based thermal strain imaging. *IEEE Transactions on Ultrasonics Ferroelectrics and Frequency Control,* vol. 52, pp. 844-850, 2005.

79. Y. Shi, F.J. de Ana, S.J. Chetcuti, M. O'Donnell. Motion artifact reduction for IVUS-based thermal strain imaging. *IEEE Transactions on Ultrasonics Ferroelectrics and Frequency Control,* vol. 52, pp. 1312-1319, 2005.